Journal of the Earth and Space Physics, Vol. 45, No. 4, Winter 2020, P. 133-142
DOI: 10.22059/jesphys.2019.275722.1007087

2-D Surface Wave Tomography in the Northwest Part of the Iranian Plateau

Zandi, H.[1] and Rahimi, H.[2*]

1. *M.Sc. Graduated, Department of Earth Physics, Institute of Geophysics, University of Tehran, Tehran, Iran*
2. Associate Professor, Department of Earth Physics, Institute of Geophysics, University of Tehran, Tehran, Iran

(Received: 16 Feb 2019, Accepted: 1 Oct 2019)

Abstract
In this study, we obtained two-dimensional tomography maps of the Rayleigh wave group velocity for the northwest part of the Iranian Plateau in order to investigate the structure of the crust and the uppermost mantle of NW Iran. To do this, the local earthquake data during the period 2006-2013, recorded by the 10 broadband stations of the Iranian seismic network (INSN) were used. After the preliminary correction, Rayleigh wave group velocity dispersion curves for each source-station path using the time-frequency analysis (FTAN) were estimated. Then, using a 2D-linear inversion procedure, the lateral variations in the group velocity distribution at different periods were calculated. The results are consistent with the previous studies and show major structural units in this region. Our results for the lower periods show distinct velocity anomalies along the North Tabriz Fault (NTF) and beneath the Sahand and Sabalan Volcanoes. Also, along the boundary of the Urumieh-Dokhtar Magmatic Arc (UDMA) and the Sanandaj-Sirjan metamorphic Zone (SSZ), lateral velocity changes are observed. The results for the longest period (the uppermost mantle) show low-velocity anomalies for most parts of the study area.

Keywords: Tomography, Rayleigh wave, Group velocity, Dispersion curves, linear inversion.

1. Introduction
The Iranian part of the Alpine-Himalayan collision zone consists of an assemblage of lithospheric blocks, features of a complex tectonic setting, which result from the collision and convergence of the Arabian plate towards Eurasia. The convergence between Arabia and Eurasia began in Late Cretaceous (Golonka, 2004). Over time, this motion led to subsequent collision stages between Arabia and smaller continental blocks resulted from the break-up of Gondwana until the final closure of Neo-Tethys Ocean. As a result of the collision between Arabian plates with Central Iran block, the Zagros-Oman-Makran orogenic system along the north-eastern margin of Arabia was built, and the Alborz and Kopet Dag were developed along the collision between Iran and the Caspian Sea and Eurasia, respectively. Because of this geodynamic evolution, a complex geological structure has formed that characterized by important lateral variations in age, composition and tectonic style (Golonka, 2004; Hatzfeld and Molnar, 2010).

Northwestern Iran is a part of the Arabia-Eurasia collision that is situated between the Caspian Sea, the southern Caucasus, the eastern Anatolia and the north of the Zagros Mountains (Figure 1). This area is a seismically active region with major deformation that is the result of the closure of the Neotethys Ocean, and the final collision of the Arabian plate with the Central Iran block. This intra-continental tectonics has begun at about 12 Ma (Copley and Jackson, 2006). Geological evidences and fault plane solution of earthquakes indicate the existence of both thrust and conjugate strike-slip faulting in this region (Talebian and Jackson, 2002; Jackson, 1992). Also, Copely and Jackson (2006) showed an unrecognized oblique normal faulting along the border northwest Iran and eastern Turkey, referred to as the Serow normal faults. One of the active fault in NW Iran is the North Tabriz fault (NTF). The NTF is part of the right-lateral fault system in the eastern Turkey-NW Iran, which partially transfers the motion across the North Anatolian and East Anatolian faults to the east, toward the Alborz and the Zagros (Moradi et al., 2010). Based on GPS data, Djamour et al. (2011) found a right-lateral strike-slip rate about 7 mm/yr for the NTF and a 250-300 years period for recurrence of earthquake for this region. Further, the two large Neogene-Quaternary volcanoes are located in this

*Corresponding author: rahimih@ut.ac.ir

region: Sahand (<0.4 Ma) and Sabalan (6.5–4.2 Ma) volcanoes, which are the dominant magmatic landscapes of NW Iran (Figure 2) (Bavali et al., 2016).

In addition to the Arabian push, the South Caspian Basin, that is an old remnant oceanic crust with a westward component of motion relative to both Eurasia and Iran, has influenced the tectonics of NW Iran as well. The velocities for the South Caspian Basin are about 8-10 mm/yr to the NW or NNW relative to Eurasia and 13-17 mm/yr to the SW relative to Iran. Because of this motion, the South Caspian is underthrusting the Talesh mountains of Iran and Azerbaijan to the west (Jackson et al., 2002).

The first studies of the crustal structure were related to the estimation of the crustal thickness beneath this region, and they suggested a crustal thickness of 45-48 km (Gheitanchi, 1996; Seber et al., 1997; Mooney et al., 1998; Bassin et al., 2000). Taghizadeh-Farahmand et al. (2010) using P and S receiver function analysis estimated Moho depths ranging between 38 km beneath the western part and about 53 km beneath the eastern part of NW of Iran. They also estimated a lithospheric thickness of about 85 km. Shad Manaman et al. (2011), using the partitioned waveform inversion (PWI) technique estimated Moho depth beneath NW Iran 40-50 and beneath the Talesh mountains 50-60 km. Mottaghi et al. (2013) based on ambient noise surface tomography for the Iranian plateau acquired the phase and group velocity maps for the periods 8-40 s.

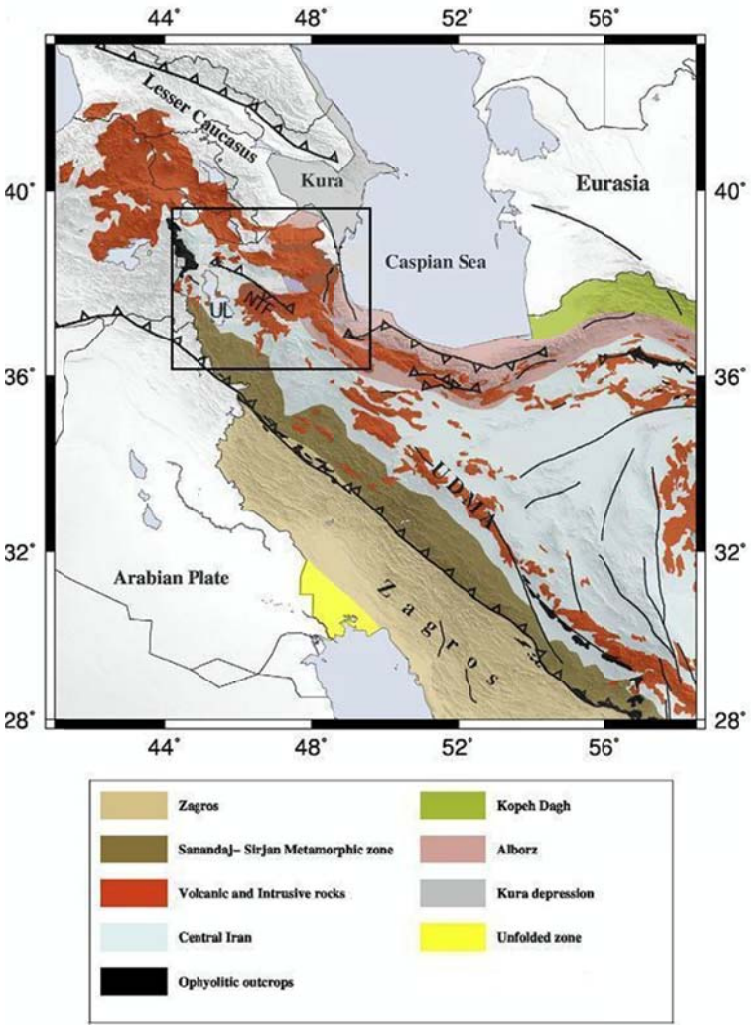

Figure 1. The main tectonic features of the Iranian Plateau (modified from Bavali et al. (2016)). The study area (Open Square) and active faults (solid lines) are shown. Abbreviations are: UL, Urumieh Lake; NTF, North Tabriz Fault; UDMA, Urumieh-Dokhtar magmatic arc.

They suggested a low velocity zone for NW Iran and along the UDMA, but for other areas of NW Iran, they indicated the high velocity structures. Maheri-Peyrov et al. (2015) obtained the M_L shear velocity for the Iranian Plateau. They showed a low shear velocity for NW Iran. Rezaeifar et al. (2016) using local earthquake tomography revealed two high and low velocity anomalies in the upper crust along the NTF. Bavali et al. (2016) using regional and teleseismic travel-time tomography obtained the lithospheric structure beneath NW Iran. They found several low-velocity anomalies in the crust and also deeper low-velocity zones in the upper mantle. In addition, they showed a high-velocity region beneath the SCB. Lü and Chen (2017) obtained the P-wave velocity structure beneath the Sahand and Sabalan Volcanoes in NW Iran. They showed low velocities in the upper crust beneath the two volcanoes. They attributed these low velocities to the upwelling of the hot materials from the mantle. Other tomographic studies of the upper mantle of the Iranian plateau (Shad Manaman et al., 2011; Lü et al., 2012; Amini et al., 2012; Mottaghi et al., 2013; Rahimi et al., 2014), and the Turkish-Iranian plateau (Hearn and James, 1994; Maggi and Priestley, 2005; Al-Lazki et al., 2004; Alinaghi et al., 2007; Al-Lazki et al., 2014) presented a low-velocity zone for the upper mantle of NW Iran.

The aim of this study is to investigate the structure of the crust and the uppermost mantle for NW Iran using surface wave tomography. To do this, we use the local earthquake data recorded by the 10 broadband stations of the INSN. The Rayleigh wave group velocity dispersion curves for each source-station path using the time-frequency analysis (FTAN), are estimated. Then, using a 2D-linear inversion method developed by Ditmar and Yanovskaya (1987) and Yanovskaya and Ditmar (1990), the 2D group velocity maps are generated. The results for the periods 5, 10, 25, and 40 s are presented. The group velocity results for the periods 2 and 50 s due to low path density (low resolution) are not presented. The results show several distinct velocity anomalies beneath the two volcanoes, along the NTF and the other structural units of the study area.

This method has not previously been used in this area. Its advantage is that it works in areas without uniformly coverage of rays. The velocity values are computed as an average of surrounding values given along the rays. The results are consistent with major geological and tectonic structures and the previous studies as well. However, the existence of a denser network of stations could be helpful in determining small-scale anomalies.

2. Data and measurements

In this study, we used the recorded local earthquakes data with magnitude greater than 2.5 that took place in NW Iran and the surrounding area during the period 2006-2013. A total of 1510 events, recorded by the 10 broadband stations of the Iranian Seismological Network (INSN) (Table 1), have been used. maximum earthquake magnitude is 6.5 and hypocentral depth for all events are less than 50 km. The study area, the locations of the epicenters of earthquakes and stations used in this study are shown in Figure 2.

Table 1. Station codes and locations of stations used in this study.

	Station Code	Longitude(˚)	Latitude(˚)	Elevation(m)
1	ASAO	50.25	34.548	**2217**
2	CHTH	51.126	35.908	**2350**
3	DAMV	51.971	35.63	**2520**
4	GHVR	51.295	34.48	**927**
5	GRMI	47.894	38.81	**300**
6	KHMZ	49.959	33.739	**1985**
7	MAKU	44.683	39.355	**1730**
8	SNGE	47.347	35.093	**1940**
9	THKV	50.879	35.916	**1795**
10	ZNJK	48.685	36.67	**2200**

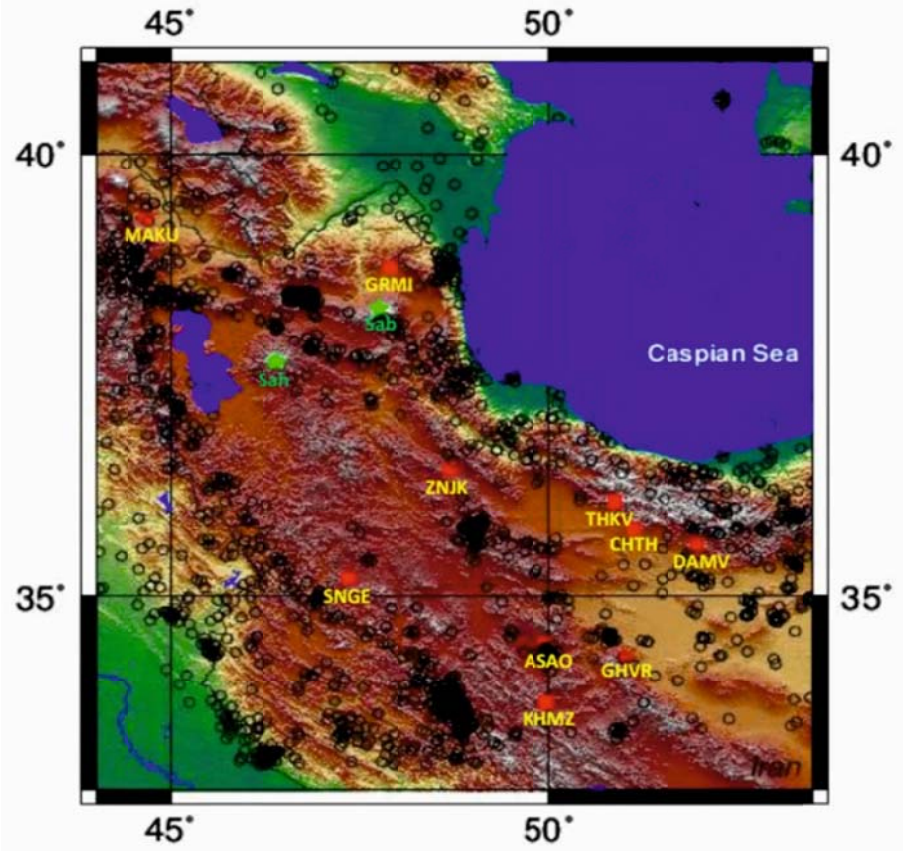

Figure 2. Map showing the study area, locations of the stations and the epicenters of events in this study. The open circles, red squares, and green stars mark earthquakes epicenters, stations, and volcanoes, respectively. Abbreviations are Sahand Volcano (Sah) and Sabalan Volcano (Sab).

The frequency-time analysis of surface waves is used to estimate the dispersion curves. After preliminary correction, for each station-earthquake pair, the group velocity dispersion curve of Rayleigh wave by applying the frequency time analysis (FTAN) method (Levshin et al., 1972, 1989, 1992) to the vertical component of motion is estimated. This method is used for estimating phase and group velocity of surface waves. It passed the preprocessed signal through a system of narrow-band filters in which the central frequency is varying. Besides, the amplitude of filter outputs is visualized in time and frequency domains. Then, on the FTAN diagram, the group velocity dispersion curve for each path is obtained. An example of the FTAN processing, for an earthquake recorded in the SNGE station is shown in Figure 3.

Finally, a set of dispersion curves for the fundamental mode Rayleigh wave in the period range from 2 to 50 s were estimated. Figure 4 shows the path coverage for period 10 s. Since estimating the dispersion curves depends on magnitude, epicentral distance, depth , etc., so different period ranges by applying FTAN to every epicenter-station pair are attained, hence for different periods we have various path numbers. Figure 5 shows the number of paths used for the tomography maps computation with respect to 11 periods. The average distance between all epicenter-station paths is of the order of 400 km.

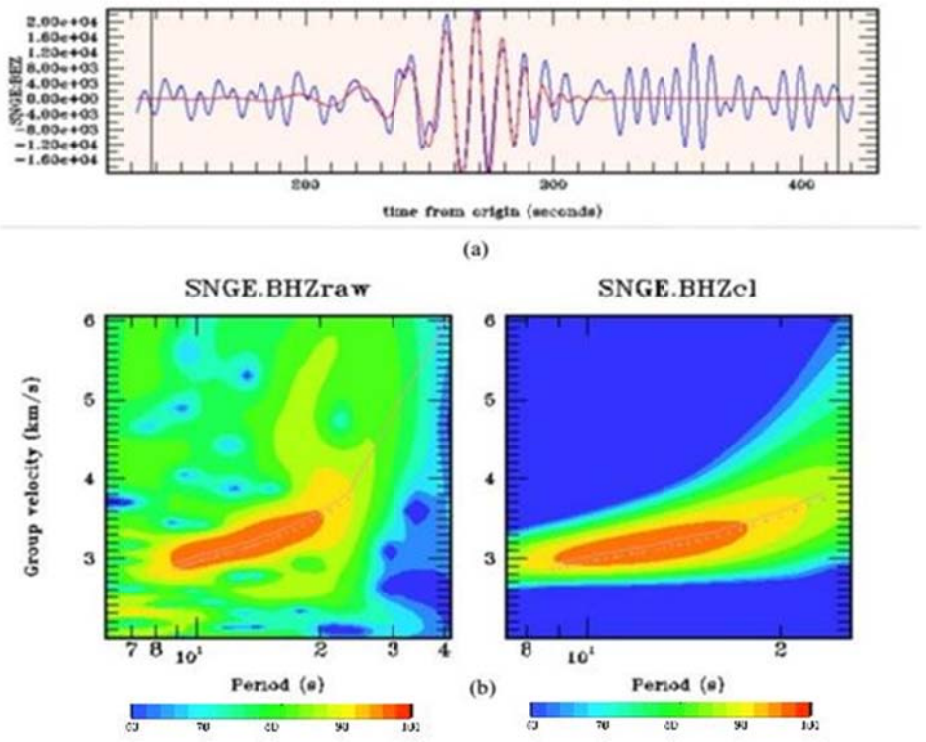

Figure 3. An example of determining group velocity dispersion curve for the vertical component of the SNGE station, for the earthquake of 13 April 2011 (Mag=3.4, Depth=5km, Dist=829.6km, Lat: 37.18, Lon: 56.202); (a) waveform records (the red line is cleaned waveform and the blue line is raw waveform); (b) FTAN diagrams for cleaned (right-hand side) and raw (the left-hand side) records. The energy contours spacing is 2 dB.

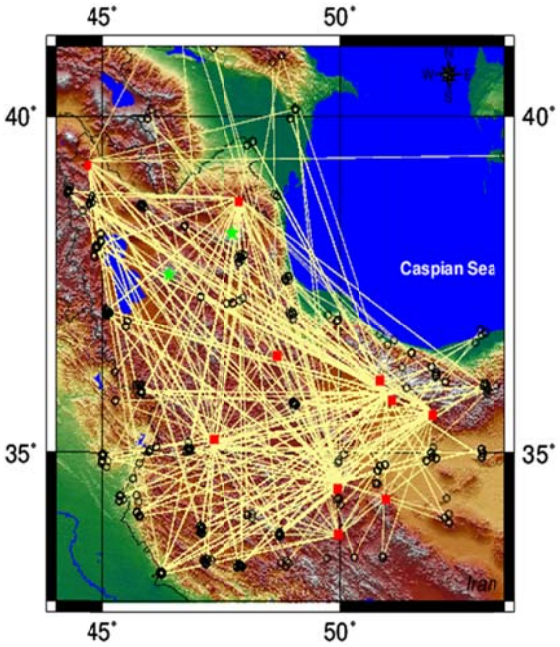

Figure 4. Path coverage of study area at period 10 s.

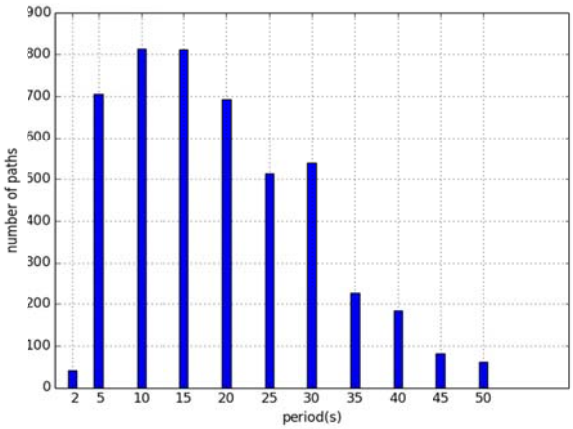

Figure 5. The number of paths according to 11 periods.

3. 2-D Tomography

Surface wave tomography became a standard procedure for imaging the heterogeneities of the earth crust and upper mantle. In this study, a 2D-linear inversion method that is developed by Ditmar and Yanovskaya (1987) and Yanovskaya and Ditmar (1990) was used to generate our group velocity maps. The

method is a generalization of the classical 1D method of Backus and Gilbert (1968). The main advantage of this method is that in the cases of uneven distribution of surface wave paths, it works well. The dataset in this method are the travel times along different paths at each period that were calculated by the frequency time analysis (FTAN). In this method, the value of the initial velocity is constant and is equal to the average velocity at a given period. The method estimates the lateral variation of group velocity $V(x)$ at each period. The lateral group velocity distribution could be estimated by minimizing the following function:

$$(\mathbf{d}-\mathbf{Gm})^T(\mathbf{d}-\mathbf{Gm})+\alpha\iint\left|\nabla m(\mathbf{x})\right|^2 d\mathbf{x}=\min, \qquad (1)$$

where:

$$m(\mathbf{x})=(V^{-1}(\mathbf{x})-V_0^{-1})V_0, \qquad (2)$$

$$d_i=t_i-t_{i0} \qquad (3)$$

$$(\mathbf{Gm})_i=\iint G_i(\mathbf{x})m(\mathbf{x})dx=\int_{l_{0i}} m(\mathbf{x})\frac{ds}{V_0} \qquad (4)$$

$$\iint G_i(\mathbf{x})d\mathbf{x}=\int_{l_{0i}}\frac{ds}{V_0}=t_{i0} \qquad (5)$$

where $x=x(\theta,\varphi)$ is the position vector, V_0 is the velocity corresponding to a starting model, t_i is the observed travel time along the i_{th} path, t_{0i} is the travel time calculated for the starting model, α is regularization parameter, t_{0i} is the length of the i_{th} path and s is the segment along which the inversion is performed. The regularization parameter that depends on the accuracy of the data, is the trade-off between the fit to the data and the smoothness of resulting velocity distribution.

Another criterion that controls the quality of the solution is the comparison between the initial mean square travel time residual and the remaining (unaccounted) residual σ. It is assumed that the unaccounted residuals are random, so σ can be accepted as an estimate of the standard error of the data, which allows a standard error of the solution σ_m to be computed. Therefore, in this study, the value of σ is used for the selection of the appropriate data: if the travel time residual for one path is larger than 3σ, this path is eliminated from the dataset and the solution is recalculated (Yanovskaya et al., 1998).

4. Group velocity maps

Since the initial data do not constrain the seismic velocities at all points of a medium, the solution to the seismic tomography problem is not non-unique. The knowledge of the resolving power of the data, therefore, can be used to estimate the minimum resolvable inhomogeneity size from the given data sample and to decide whether or not, features of the solution could possibly be artifacts due to the specific solution method. Yanovskaya (1997) and Yanovskaya et al. (1998) proposed the use of two parameters to evaluate lateral resolution: the mean size and the stretching of the averaging area.

In this tomography method, the velocities are calculated as an average of the surrounding values given along the rays. Therefore, the method has a variable number of grid nodes where the velocity values are estimated, and it not only gives the velocity distribution, but also permits to see the averaging area for each grid node. Therefore, the mean size (the resolution length) and stretching of this averaging area are an estimation of the resolution in every point. In the case that there is only sparse ray coverage, the mean size averaging area is larger. In contrast, in the case that ray coverage is good and also the distribution of rays is uniform, the resolution is better. The values of the 'stretching' parameter indicate the distribution of paths. Small values of this parameter indicate uniform distribution along all directions, and large values of that (usually>1) mean that the paths have a preferred orientation, and so, the resolution along this direction is small (Yanovskaya, 1997; Yanovskaya et al., 1998).

An important factor that controls the tomography results is the regularization parameter. The results and their reliability are easily compared by different regularization parameters and grid node distributions. The higher values of this parameter results in a smoother group velocity distribution and larger residuals and hence a larger averaging area for each grid node. For Smaller values of the parameter, group velocity distributions are very perturbed and, thus, averaging areas

and residuals are smaller, that theoretically leads to a better resolution but a large solution error. Therefore, for an improving in the resolution and having a real model we tested various values of the regularization parameter. Finally, we choose $a = 0.2$ that gives relatively smooth maps with small solution errors.

Rayleigh wave group velocity maps for the period range 2-50 s were produced. The size of each cell for the resulting maps was $0.5^{\circ} \times 0.5^{\circ}$ $(\sim 50km)$. The group velocity maps, the standard error values of local group velocity, resolution length (the mean size of the averaging area), and stretching parameter at periods 5, 10, 25, and 40 s are shown in Figure 6.

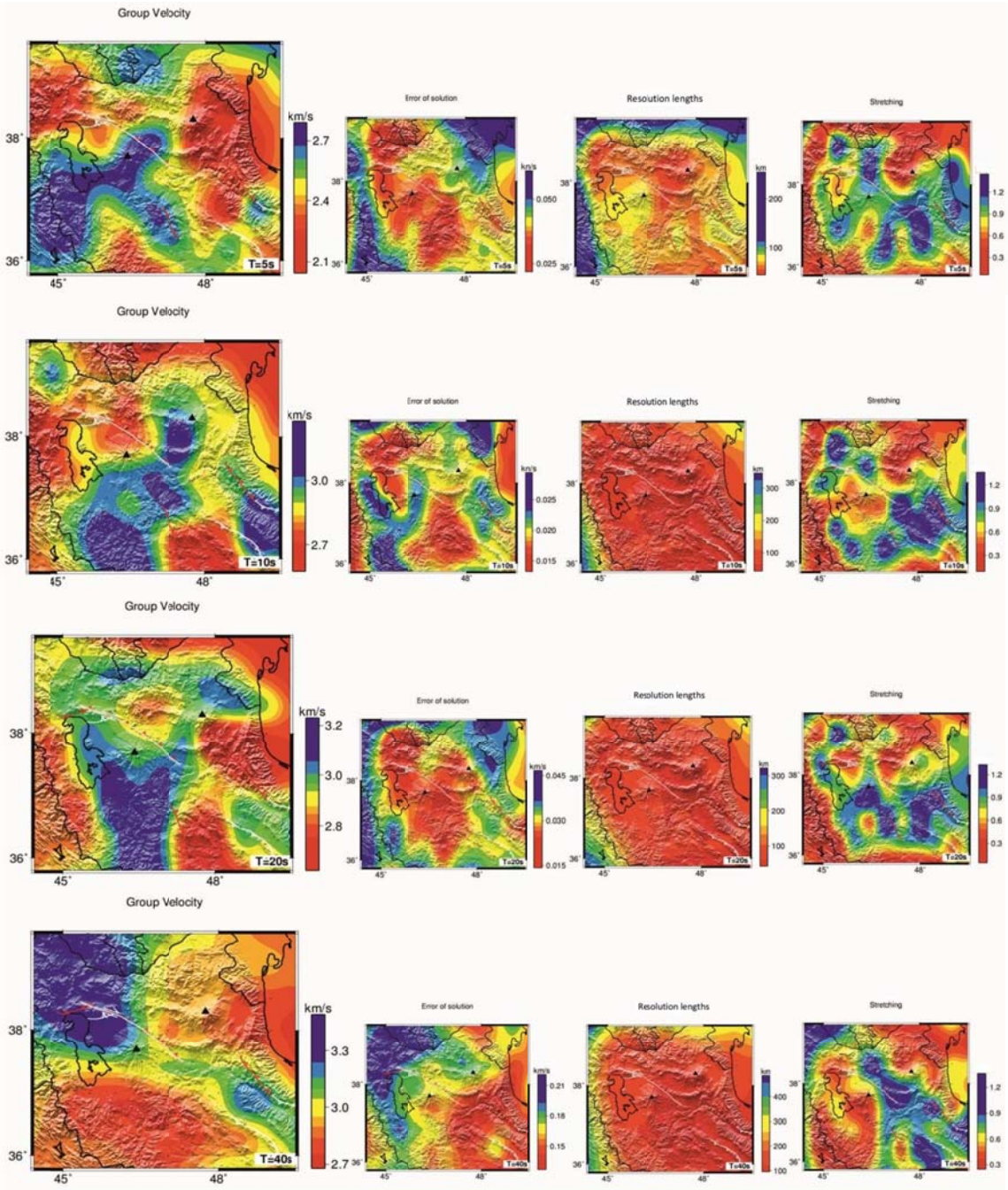

Figure 6. Rayleigh-wave group velocity tomography maps, the error of solution, resolution lengths, and stretching parameter at periods 5, 10, 20, and 40 s.

5. Discussion and conclusions

Certainly, the dispersion measurements are not free of uncertainty because of the source mislocation. Chen et al. (2010) analyzed this problem and found the statistical margin of error due to source mislocation that is less than 0.03 km/s for Rayleigh waves velocity. The error value for the parts of the study area that has a low ray coverage is higher and marked with blue color. It ranges from 0.015 to 0.05 km/s, but for most parts of the study area, it is less than 0.03 km/s. The values of group velocities at each grid are calculated as the mean of the velocity data along different paths. In case that path coverage is poor, the size of resolution length is large. The resolution lengths in the eastern parts are lower (marked with red color), so we have a high resolution for these parts. The dimensions of heterogeneities can be determined from the resolution length maps. The resolution length results are on the order of 50-150 km for the most parts of the study area, but for the marginal areas with low ray coverage, these values are even more. The stretching parameter values are spatial distribution (azimuthal coverage) of the paths, and large values of this parameter show a preferred orientation of the paths. The distribution of the stations and earthquakes controls the stretching parameter. The smaller value of that (usually <1) indicates a uniform distribution of rays. Its values in our results are about 0.8 that shows a uniform distribution and an identical resolution along each path for most parts of the study area (Figure 6).

The results show a good agreement with the dominant geological structures and the previous studies. The Rayleigh group velocity range at period of 5 s is from 2.1 to 2.8 km/s and has an average of 2.4 km/s. Rezaeifar et al. (2016) showed two distinct velocity anomalies that extend to the depth 14 km with their boundaries parallel to the NTF: a high velocity anomaly related to basaltic volcanic rocks in the south and a low velocity anomaly related to sedimentary rocks in the north of the NFT. These high and low velocities are observed in our group velocity results at periods 5 s (depth about 6 to 8 km) and 10 s (depth about 15 km). Also, our results at period of 5 s show a low velocity zone beneath the Sabalan Volcano, which could be due to the high temperature of the volcanic rocks or shallow magma chamber beneath this volcano. The existence of the hot springs around this volcano signify this high temperature rocks. Beneath the Sahand Volcano a high velocity zone is observed that could be due to a low temperature volcanic rocks or a deeper magma chamber. Another distinct high velocity zone is observed for the southwestern areas that could be attributed to the Mesozoic volcanic rocks (along the SSZ). The group velocity range at period 10 s is from 2.6 to 3.3 km/s and has an average of 2.9 km/s. At period of 10 s, the results are different (depth about 15 km). A relatively low velocity zone beneath the Sahand Volcano is observed that extends to the north. Also, a high velocity zone beneath the Sabalan Volcano that may indicate a transition from warm magmatic rocks to colde ones. Along the SSZ a high velocity zone is observed as well, which can be related to the sedimentary and metamorphic Paleozoic-Cretaceous rocks in this zone. While along the UDMA a low velocity zone is observed that could be due to volcanic and sedimentary rocks that reflect the lava flows through the pyroclastic deposits of the upper crust along the zone of UDMA (Mottaghi et al., 2013). The group velocity at period of 20 s (depth about 32 km) has an average of 2.9 km/s. The results at period of 20 s show a low velocity anomaly for the eastern areas and along the UDMA. However, in the southwest areas (along the SSZ), a high velocity zone is observed. Mottaghi et al. (2013) showed a high velocity zone beneath the SSZ and a low velocity zone beneath the UMDA, and they also showed a low velocity zone at period of 32 s beneath the SSZ and the UMDA. The group velocity range at period of 40 s is from 2.7 to 3.5 km/s and has an average of 3.1 km/s. The results at period of 40 s are different, for the southern areas show low group velocities, while, for the northern areas show higher group velocities, and these could be due to the difference in the crust structure such as thickness and type of the lower parts of the crust and the uppermost mantle. The previous studies showed a low velocity zone for the uppermost mantle in the NW Iran (Hearn and James, 1994; Al-Lazki et al., 2004; Maggi

and Priestley, 2005; Alinaghi et al., 2007; Tabatabai et al., 2008; Shad Manaman et al., 2011; Amini et al., 2012; Al-Lazki et al., 2014; Bavali et al., 2016).

In this study, the 2D Rayleigh wave group velocity maps in the period's 5-40 s for NW Iran were obtained. The results correspond to the major structural units. At period of 5 s, a low velocity zone beneath the Sabalan Volcano is observed that is most likely related to a shallow thermal origin. Beneath the Sahand Volcano in the south of the NTF a high velocity zone is observed, whereas for the sedimentary rocks in the north of the NTF a low velocity zone is observed. At periods of 10 and 20 s, a relatively low velocity zone beneath the Sahand Volcano is observed that extends to the north. This shows a deeper thermal source beneath the Sahand Volcano than the Sabalan Volcano. Moreover, lateral velocity changes along the Boundary of the UDMA and the SSZ (at periods 5, 10, and 20 s) are observed, which corresponds to the suture zone found along the boundary of the UDMA and the SSZ (Mottaghi et al., 2013). The results at period of 40 s (the uppermost mantle) show a relatively low group velocity for most parts of the study area that could be due to the warm upper mantle in NW Iran. However, determining the source of the high velocity anomaly at period 40 s due to low resolution (low resolution lengths) is difficult.

References

Alinaghi, A., Koulakov, I. and Thybo, H., 2007, Seismic tomographic imaging of P- and S-waves velocity perturbation in the upper mantle beneath Iran, Geophys. J. Int., 169, 1089-1102.

Al-Lazki, A.I., Sandvol, E., Seber, D., Barazangi, M., Turkelli, N. and Mohamad, R., 2004, Pn tomographic imaging of mantle lid velocity and anisotropy at the junction of the Arabian, Eurasian and African plates, Geophys. J. Int., 158, 1024–1040.

Al-Lazki, A.I., Al-Damegh, K.S., El-Hadidy, S.Y., Ghods, A. and Tatar, M., 2014, Pn velocity structure beneath Arabia–Eurasia Zagros collision and Makran subduction zones, Geological Society, London, Special Publications, 392(1), 45–60.

Amini, S., Shomali, Z.H., Koyi, H. and Roberts, R.G., 2012, Tomographic upper-mantle velocity structure beneath the Iranian Plateau, Tectonophysics, 554-557, 42-49.

Backus, G.E. and Gilbert, J.F., 1968, The resolving power of gross Earth data. Geophys. J. R. Astr. Soc., 16, 168-205.

Bassin, C., Laske, G. and Masters, G., 2000, The current limits of resolution for surface wave tomography in North America, EOS. Trans. AGU, 81, F897.

Bavali, K., Motaghi, K., Sobouti, F., Ghods, A., Abbasi, M., Priestley, K., Mortezanejad, G. and Rezaeian, M., 2016, Lithospheric structure beneath NW Iran using regional and teleseismic travel-time tomography, Physics of the Earth and Planetary Interiors, 253, 97–107.

Chen, Y., Badal, J. and Hu, J., 2010, Love and Rayleigh wave tomography of the Quighai-Tibet plateau and surrounding areas, Pure Appl. Geophys., 167(10), 1171-1203.

Copley, A. and Jackson, J., 2006, Active tectonics of the Turkish-Iranian Plateau, Tectonics, 25, TC6006.

Ditmar, P.G. and Yanovskaya, T.B., 1987, Generalization of Backus-Gilbert Method for Estimation of Lateral Variations of Surface wave Velocities, Phys. Solid Earth, Izvestia Acad. Sci. USSR, 23(6), 470-477.

Djamour, Y., Vernant, P., Nankali, H.R. and Tavakoli, F., 2011, NW iran-eastern Turkey present-day kinematics: Results from the Iranian permanent GPS network, Earth and Planetary Science Letters, 307, 7-34.

Gheitanchi, M.R., 1996, Crustal structure in Nw in Iran, revealed from the 1990 Rudbar aftershock sequence, J. Earth Space Phys., 23, 7-14.

Golonka, J., 2004, Plate tectonic evolution of the southern margin of Eurasia in the Mesozoic and Cenozoic, Tectonophysics, 381, 235-273.

Hatzfeld, D. and Molnar, P., 2010, Comparisons of the kinematics and deep structures of the Zagros and Himalaya and of the Iranian and Tibetan Plateaus and geodynamics implications, Rev. Geophysics., 48, RG2005, doi:10.1029/2009RG000304.

Hearn, T.M. and James, F.NI. 1994, Pn

velocities beneath continental collision zones: the Turkish-Iranian Plateau, Geophys. J. Int., 117, 273-283.

Jackson, J., 1992, Partitioning of strike-slip and convergent mountain between Eurasia and Arabian in Eastern Turkey and the Caucasus, J. Geophys. Res., 97, 12471-12479.

Jackson, J., Priestley, K., Allen, M. and Berberian, M., 2002, Active tectonics of the South Caspian Basin, Geophys. J. Int., 148, 214-245.

Levshin, A.L., Ratnikova, L.I. and Berteussen, K.A., 1972, On a frequency-time analysis of oscillations, Ann. Geophys., 28, 211-218.

Levshin, A.L., Yanovskaya, T.B., Lander, A.V., Bukchin, B.G., Barmin, M.P.M., Ratnikova, L.I. and Its, E.N., 1989, Recording, identification and measurements of surface wave parameters, In: Keilis-borok, V.I. (Ed.), Seismic Surface Waves in a Laterally Inhomogeneous Earth, Kluwer Academic Publishing, Dordrecht, 131-182.

Levshin, A.L., Ratnikova, L.I. and Berger, J., 1992, Peculiarities of surface-wave propagation across central Eurasia, Bull. Seimol. Soc. Am., 82, 2464-2493.

Lü, Y. and Chen, L., 2017, Upper crustal P-wave velocity structure beneath two volcanic areas in northern Iran, Sci. China Earth Sci., 60, 786-795.

Lü, Y., Liu, B., Pei, S., Sun, Y., Toksöz, M.N. and Zeng, X., 2012, Pn tomographic velocity and anisotropy beneath the Iran region, Bull. Seismol. Soc. Am., 102(1), 426– 435.

Maggi, A. and Priestley, K., 2005, Surface waveform tomography of the Turkish-Iranian plateau, Geophys. J. Int., 160, 1068-1080.

Maheri-Peyrov, M., Ghods, A., Abbasi, M., Bergman, E. and Sobouti, F., 2015, M_L shear wave velocity tomography for the Iranian Plateau, Geophys. J. Int., 205, 179-191.

Mooney, W.D., Laske, G. and Masters, G., 1998, Crust-5.1: A global crustal model at 5×5 degrees, J. Geophys. Res., 103, 727-747.

Moradi, A.S., Hatzfeld, D. and Tatar, M., 2011, Microseismicity and seismotectonics of the North Tabriz fault (Iran), Tectonophysics, 506(1), 22-30.

Mottaghi, A., Rezapour, M. and Korn, M., 2013, Ambient noise surface wave tomography of the Iranian Plateau, Geophys. J. Int., 193, 452–462.

Rahimi, H., Hamzehloo, H., Vaccari, F. and Panza, G.F., 2014, Shear-wave velocity tomography of the lithosphere-asthenosphere system beneath the Iranian Plateau, Bulletin of the Seismological Society of America, 104(6).

Rezaeifar, M., Kissling, E., Shomali, Z.H. and Shahpasand-Zadeh, M., 2016, 3D crustal structure of the northwest Alborz region (Iran), Swiss J. Geosci, 109(3), 389-400.

Seber, D., Vallve, M., Sandvol, E., Steer, D. and Barazangi, M., 1997, Middle East tectonics: application of geographic information systems (GIS). GSA Today, 7(2), 1-6.

Shad Manaman, N., Shomali, H. and Koyi, H., 2011, New constraints on upper-mantle S-velocity structure and crustal thickness of the Iranian plateau using partitioned waveform inversion, Geophys. J. Int., 184, 247-267.

Taghizadeh-Farahmand, F., Sodoudi, F., Afsari, N. and Ghassemi, M.R., 2010, Lithospheric structure of NW Iran from P and S receiver functios, J. Seismol. 14, 823-836.

Talebian, M. and James, J., 2002, Offset on the Main Recent Fault of NW Iran and implications for the late Cenozoic tectonics of the Arabic-Eurasia collision zone, Geophys. J. Int., 150, 422-439.

Yanovskaya, T.B. and Ditmar P.G., 1990, Smoothness criteria in surface wave tomography, Geophys. J. Int., 102, 63-72.

Yanovskaya, T.B., 1997, Resolution estimation in the problems of seismic ray tomography, Izv. Phys. Solid Earth, 33 (9), 762-765.

Yanovskaya, T.B., Kizima, E.S. and Antonova, L.M., 1998, Structure of the crust in the Black Sea and adjoining regions from surface wave data, J. Seismol., 2, 303-316.